Smart Mater. Struct. **17** (2008) 065020 (10pp) doi:10.1088/0964-1726/17/6/065020

Nonlinear elastic modeling of differential expansion in trilayer conjugated polymer actuators

Yang Fang[1], **Thomas J Pence**[2] **and Xiaobo Tan**[1,3]

[1] Smart Microsystems Laboratory, Department of Electrical and Computer Engineering, Michigan State University, East Lansing, MI 48824, USA
[2] Department of Mechanical Engineering, Michigan State University, East Lansing, MI 48824, USA

E-mail: fangyang@msu.edu, pence@egr.msu.edu and xbtan@msu.edu

Received 18 May 2008, in final form 16 September 2008
Published 22 October 2008
Online at stacks.iop.org/SMS/17/065020

Abstract
Conjugated polymers are promising actuation materials for biomimetic robots and biomedical devices. Large bending is involved in some of these applications. This poses significant challenges in electromechanical modeling, because the linear elasticity theory is only valid when the strain is small. In this paper an effective strategy based on the nonlinear elasticity theory is proposed to model the mechanical output of a trilayer conjugated polymer beam under actuation. Instead of using the elastic modulus as in the linear elasticity theory, we use a nonlinear strain energy function to capture the stored elastic energy under actuation-induced swelling, which further allows us to compute the induced stress. The deformation variables are obtained by numerically solving the force and bending moment balance equations simultaneously. Experimental results have demonstrated that the proposed model shows superiority over the linear model, and is able to capture the actuation behavior well under large actuation voltages. The proposed framework can also be applied to the analysis of large deformations in some other electroactive polymers.

(Some figures in this article are in colour only in the electronic version)

1. Introduction

Electroactive polymers (EAPs) are promising actuation and sensing materials with potential applications in robotics and biomedical systems [1–6]. One class of EAP materials is conjugated polymers or conducting polymers [7–9]. Polypyrrole (PPy) and polyaniline (PANI) are two of the most commonly used conjugated polymers for actuation purposes. The backbones of conjugated polymers have alternating single and double carbon–carbon bonds (conjugation), which results in positive charge carriers and thus electrical conductivity. The electrons can be removed from the polymers electrochemically by applying a sufficiently positive potential (oxidation), during which negatively charged anions can be incorporated into the polymer backbone to maintain the charge neutrality. Application of a sufficiently negative potential can reverse the process and repel the trapped anions out of the polymer (reduction). Volumetric change (swelling) introduced by the mass transport of ions during reduction/oxidation is considered to be the primary mechanism of actuation [8]. One advantage of conjugated polymer actuators is that they can generate large swelling under low actuation voltages. The strains generated by PPy actuators are typically between 1% and 10% [7, 10]. A 20% contraction was observed in the thickness direction of a PANI film [11]. Conjugated polymer actuators have numerous potential applications, such as microfluidic pumps [12], blood vessel connectors [13], and microvalves for flow control [14]. Different configurations of actuators have been exploited for these applications, e.g., bilayer benders [1], trilayer benders [15, 16], and linear extenders [7, 10].

It is important to model the sophisticated electrochemical mechanism of conjugated polymer actuators for precise control of their force and/or displacement output in many of the envisioned applications. A complete model can generally be

[3] Author to whom any correspondence should be addressed.

divided into two major components. The first component is to understand the dynamic relationship between the amount of transferred ions and the applied potential. There has been extensive modeling work on this, such as the 'diffusive-elastic-metal' model [17], which considers diffusion as the dominant mechanism of ion movement. The second component is to predict the mechanical output based on the swellings introduced by the transferred ions. The classical beam theory has been used to model the bending curvature for bilayer PPy actuators [18, 19] and trilayer actuators [20]. However, the model is only valid when the ion movement-induced swelling is small so that the following two assumptions hold: (1) the strain and the stress can be related linearly; (2) the geometry nonlinearities can be neglected. Alici and co-workers modeled the bending curvature and force output for trilayer PPy actuators by using finite element analysis in analogy with a thermally driven beam, but no analytical model was presented [21]. Tensile strength experiments have shown that the strain and stress relationship of PPy film becomes clearly nonlinear as the strain is increased over 4% [22, 23]. These results indicate that the linear model based on the assumption that the stress varies linearly with the strain becomes invalid as the deformation gets large. Therefore, it is imperative to develop a nonlinear model to predict the actuator performance for applications in which large actuation is involved.

In this paper, a nonlinear elasticity-based method is proposed to capture the mechanical deformation induced by transferred ions. A trilayer PPy actuator, which has two PPy layers sandwiching an amorphous polyvinylidene fluoride (PVDF) layer, is used as an example to illustrate the framework of the analysis. Neo-Hookean type strain energy functions are used for both PPy and PVDF to capture the nonlinear stress–strain relationship, which incorporates the effect of swelling [24]. The actuation-induced stresses are derived from the strain energy functions. The equilibrium configuration under a quasi-static actuation voltage is then obtained by solving the force and moment balance equations simultaneously. Experiments have been conducted to verify the effectiveness of the proposed model. For comparison purposes, a linear elasticity theory-based model is also used. When the applied voltages are small, the predictions by both models are close to experimental data. But the nonlinear elasticity model fits the experimental data better as the input voltage increases, which shows the superiority of the method in modeling large deformations of conjugated polymers.

The remainder of the paper is organized as follows. In section 2, the electrical impedance module and electromechanical coupling are first introduced. Then the derivation of the mechanical model based on the nonlinear elasticity theory is presented in section 3. Experimental setups are described in section 4. The results are discussed in section 5. Conclusions are provided in section 6.

2. Review of a linear model

The working principle of a trilayer PPy actuator is illustrated in figure 1. In the middle is an amorphous, porous polyvinylidene fluoride (PVDF) layer that serves as both a backing material and a storage tank for the electrolyte. On both sides of the actuator are the PPy layers. When a voltage is applied across the actuator, the PPy layer on the anode side is oxidized while the other layer on the cathode side is reduced. The oxidized layer absorbs anions and expands, while the reduced layer gives up anions and contracts. The differential expansion thus leads to bending of the actuator, as shown in figure 1.

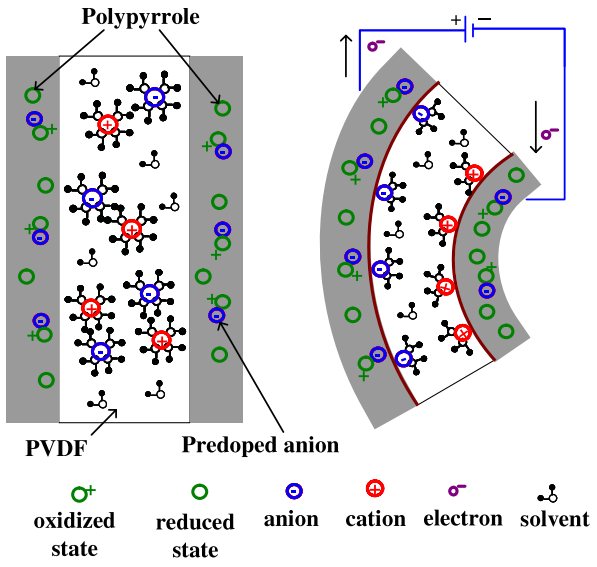

Figure 1. Illustration of the actuation mechanism of a trilayer polypyrrole actuator. Left: a sectional view of the trilayer structure; right: bending upon application of a voltage.

In this section, a linear model for the trilayer conjugated polymer actuator will be reviewed. The model has three cascaded modules: (1) the electrical admittance module, (2) the electromechanical coupling module, and (3) the mechanical module. While the first and second modules are adopted in the current work, the third module will be replaced by a nonlinear elasticity theory-based module.

2.1. Electrical admittance module

As the first step to model the electrochemomechanical phenomenon, the admittance model is important; it characterizes the relationship between the current through the polymer and the actuation voltage. One can integrate the current to obtain the amount of the transferred ions and furthermore calculate the swelling of the polymer. A diffusive-elastic-metal model is proposed for PPy based on the Randles equivalent circuit model, in which the ion transport within the polymer is determined by the diffusion law [17, 25]. The admittance model in the Laplace domain is

$$\frac{I(s)}{U(s)} = \frac{s[\frac{\sqrt{D}}{\delta}\tanh(h\sqrt{s/D}) + \sqrt{s}]}{\frac{\sqrt{s}}{C} + Rs^{3/2} + R\frac{\sqrt{D}}{\delta}s\tanh(h\sqrt{s/D})}, \tag{1}$$

where s is the Laplace variable, D is the diffusion coefficient, δ is the thickness of the double layer at the polymer/electrolyte interface, h is the thickness of each PPy layer, C denotes the double-layer capacitance, and R is the electrolyte and

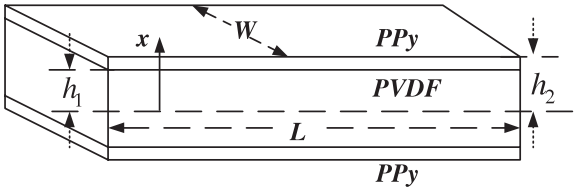

Figure 2. Definitions of parameters used in the linear mechanical model.

contact resistance. When a DC voltage U is applied across the polymer, the total transferred charges can be calculated by using the Final Value Theorem [26] on (1):

$$Q = k_1 U, \tag{2}$$

where $k_1 = \frac{1}{2}(1 + \frac{h}{\delta})C$. This means that the amount of transferred charges at the steady state is proportional to the applied voltage. The proportionality constant can be calculated based on the fundamental parameters or measured directly from the experiments. In this paper, the experimental method is used to obtain the value of k_1 for different samples.

2.2. Electromechanical coupling module

The ions transferred to the polymer cause expansion of the polymer. It has been observed that the volume change can be captured by $k_2\rho$, where k_2 is the swelling-to-charge ratio and ρ is the density of the transferred charges [17, 18]. In order to obtain ρ, the transferred charge Q is obtained by integrating the current, which consists of a component due to ion diffusion into the PPy layer and a component due to double-layer charging [17]. Because the bulk capacitance of the PPy is much larger than the double-layer capacitance, the charges in the double layer at the steady state are negligible compared to that in the bulk of PPy [20]. Therefore the transferred charge density ρ is

$$\rho = \frac{Q}{V}, \tag{3}$$

where V is the volume of the PPy layer.

2.3. Linear mechanical model

The bending of the trilayer beam can be predicted based on the linear elasticity theory after the swelling ratios are determined for different layers. One key assumption for the linear model is that the relationship between the stress and strain is linear, given by the small strain Young's modulus, which is reasonable when the strain is sufficiently small. The elastic strain is obtained through the elementary beam theory by assuming that the strain changes linearly in the thickness direction with the distance from an appropriately located neutral line in the thickness direction [27] (represented by x in figure 2):

$$\varepsilon(x) = \kappa x, \tag{4}$$

where κ is the curvature to be determined.

When there is no external load, the beam curvature can be obtained by solving the force and moment balance equations simultaneously:

$$\int_{-h_2}^{-h_1} \sigma_{\mathrm{PPy1}}(x)\,\mathrm{d}x + \int_{-h_1}^{h_1} \sigma_{\mathrm{PVDF}}(x)\,\mathrm{d}x + \int_{h_1}^{h_2} \sigma_{\mathrm{PPy2}}(x)\,\mathrm{d}x = 0, \tag{5}$$

$$\int_{-h_2}^{-h_1} \sigma_{\mathrm{PPy1}}(x)x\,\mathrm{d}x + \int_{-h_1}^{h_1} \sigma_{\mathrm{PVDF}}(x)x\,\mathrm{d}x + \int_{h_1}^{h_2} \sigma_{\mathrm{PPy2}}(x)x\,\mathrm{d}x = 0, \tag{6}$$

where h_1 and h_2 are as defined in figure 2. By superimposing the bending effect term upon the swelling term, the normal stresses in the PPy and PVDF layers along the beam direction are taken to be

$$\sigma_{\mathrm{PPy1}}(x) = E_{\mathrm{PPy}}\varepsilon(x) - E_{\mathrm{PPy}}k_2\rho, \tag{7}$$

$$\sigma_{\mathrm{PVDF}}(x) = E_{\mathrm{PVDF}}\varepsilon(x), \tag{8}$$

$$\sigma_{\mathrm{PPy2}}(x) = E_{\mathrm{PPy}}\varepsilon(x) + E_{\mathrm{PPy}}k_2\rho, \tag{9}$$

where E_{PPy} and E_{PVDF} are the small strain Young's moduli of the PPy and PVDF, and PPy1 and PPy2 represent the reduced and oxidized PPy layers, respectively. For a symmetrical trilayer actuator, with the assumption that the thickness of the two PPy layers remains constant, it follows from (5) that the neutral line is the beam center line. Therefore, the actuation-induced curvature κ can be evaluated from (6) and the free-bending response is obtained by combining (1), (3), and (6):

$$\frac{\kappa(s)}{U(s)} = \gamma_m \frac{\frac{\sqrt{D}}{\delta}\tanh(h\sqrt{\frac{s}{D}}) + \sqrt{s}}{\frac{\sqrt{s}}{C} + Rs^{3/2} + R\frac{\sqrt{D}}{\delta}s\tanh(h\sqrt{\frac{s}{D}})}, \tag{10}$$

where γ_m is defined as

$$\gamma_m \triangleq \frac{3k_2[(1+\frac{h_2-h_1}{h_1})^2 - 1]}{2h_1WL(h_2-h_1)[(1+\frac{h_2-h_1}{h_1})^3 + \frac{E_{\mathrm{pvdf}}}{E_{\mathrm{ppy}}} - 1]}.$$

Although (10) is only used later for steady-state analysis, it is provided here to give a complete description of the actuation mechanism. It will also be useful in the future, when dynamic deformation is considered. Note that one can incorporate the viscoelasticity of the materials by using frequency-dependent Young's moduli for PPy and PVDF [28]. When a DC voltage U is applied across the polymer, the steady-state curvature is obtained based on (2):

$$\kappa = \gamma_m k_1 U. \tag{11}$$

3. Nonlinear mechanical model based on a swelling framework

Large swelling and bending present challenges to the mechanical model based on the linear elasticity theory. Firstly, when the deformation is large, the swelling effect and the bending effect are coupled and thus cannot be superimposed as those in (7) and (9) due to the geometric nonlinearities.

Secondly, the strain–stress relationship of PVDF and PPy films becomes nonlinear as the strain increases [22, 23, 29, 30]. Thirdly, under large swelling, the symmetrical trilayer arrangement generates a neutral line that is no longer at the center line due to the geometric nonlinearity. Therefore, the nonlinear elasticity theory-based method is introduced in this section to model large bending motions.

3.1. Definition of swelling

We use ν_1 and ν_2 to denote the swellings of the reduced and oxidized PPy layer, respectively. The swelling is defined as the ratio between the volume after electrical actuation and the original volume. If $\nu_i > 1$, the volume is increased; if $\nu_i < 1$, the volume is decreased. Assuming that the volume change is proportional to the transferred charge density, one can calculate ν_1 and ν_2 at the steady state:

$$\nu_1 = \frac{V_0 - k_2 \rho V_0}{V_0} = 1 - k_2 \rho, \tag{12}$$

$$\nu_2 = \frac{V_0 + k_2 \rho V_0}{V_0} = 1 + k_2 \rho, \tag{13}$$

where V_0 represents the original volume. The value of k_2 can be determined by experimental data; it has the order of 10^{-10} m^3 C^{-1} [17]. When one PPy layer is reduced and repels dopants, the other PPy layer is oxidized and accepts dopants. Therefore, the PVDF layer is merely an ion conducting layer, and we assume that its volume does not change.

3.2. Finite strain tensors

In linear elasticity the infinitesimal strain tensor is used to capture the structural deformation, where 'infinitesimal' implies that the theory is only valid as the displacement gradient is vanishingly small. However, the strain can be significant in many applications. Thus the finite strain tensors are introduced in nonlinear elasticity, which will be adopted below.

Consider a trilayer beam that bends because of differential swellings in the two outer layers. The reference configuration is in Cartesian coordinates, while the deformed configuration is in cylindrical coordinates for the convenience of modeling the bending. This is shown in figure 3, where x represents the thickness coordinate, y represents the length coordinate, and z stands for the width coordinate. The axes in the cylindrical coordinates are labeled by r, θ, and ς, which represent the radius, azimuth, and width coordinates, respectively. Because the length of the beam is usually much larger than the width, it is assumed that there are no changes along the width direction z, which means

$$\varsigma = z. \tag{14}$$

The bending angle θ is considered to be proportional to the position along the y axis in the reference configuration,

$$\theta = \alpha y, \tag{15}$$

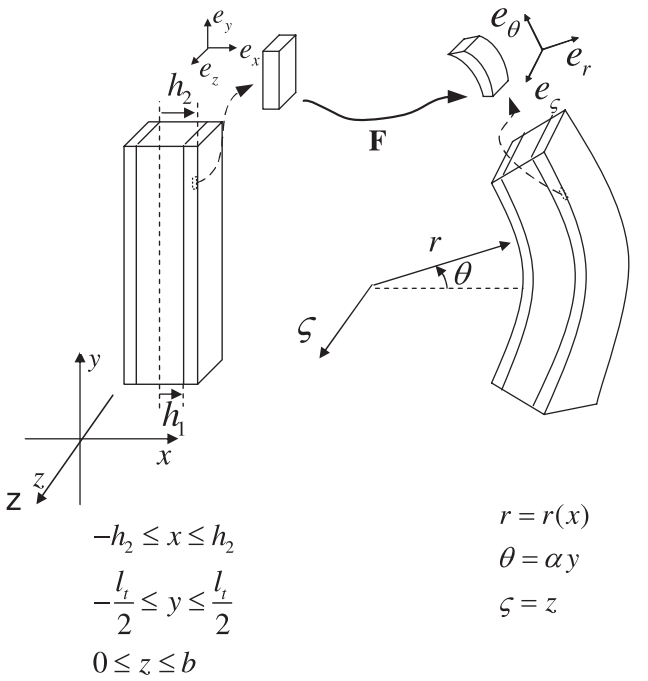

Figure 3. Illustration of the reference configuration and the deformed configuration.

where α is a proportionality constant that will be determined by the analysis. The bending radius r is assumed to be independent of y and z,

$$r = r(x). \tag{16}$$

The orthonormal basis vectors in the Cartesian coordinates are denoted by $\mathbf{e_x}$, $\mathbf{e_y}$, and $\mathbf{e_z}$, and they are denoted by $\mathbf{e_r}$, $\mathbf{e}_\theta$, and $\mathbf{e}_\varsigma$ in the cylindrical coordinates. By definition, these vectors are represented by

$$\mathbf{e_x} = \begin{pmatrix} 1 \\ 0 \\ 0 \end{pmatrix}, \qquad \mathbf{e_r} = \begin{pmatrix} 1 \\ 0 \\ 0 \end{pmatrix},$$
$$\mathbf{e_y} = \begin{pmatrix} 0 \\ 1 \\ 0 \end{pmatrix}, \qquad \mathbf{e}_\theta = \begin{pmatrix} 0 \\ 1 \\ 0 \end{pmatrix},$$
$$\mathbf{e_z} = \begin{pmatrix} 0 \\ 0 \\ 1 \end{pmatrix}, \qquad \mathbf{e}_\varsigma = \begin{pmatrix} 0 \\ 0 \\ 1 \end{pmatrix}.$$

For ease of analysis, the dyadic product is denoted by the symbol $\bigotimes$. It operates as follows:

$$\begin{pmatrix} x_1 \\ x_2 \\ x_3 \end{pmatrix} \otimes \begin{pmatrix} y_1 \\ y_2 \\ y_3 \end{pmatrix} = \begin{pmatrix} x_1 y_1 & x_1 y_2 & x_1 y_3 \\ x_2 y_1 & x_2 y_2 & x_2 y_3 \\ x_3 y_1 & x_3 y_2 & x_3 y_3 \end{pmatrix}. \tag{17}$$

This gives the matrix representations

$$\mathbf{e_r} \otimes \mathbf{e_x} = \begin{pmatrix} 1 & 0 & 0 \\ 0 & 0 & 0 \\ 0 & 0 & 0 \end{pmatrix}, \tag{18}$$

$$\mathbf{e}_\theta \otimes \mathbf{e_y} = \begin{pmatrix} 0 & 0 & 0 \\ 0 & 1 & 0 \\ 0 & 0 & 0 \end{pmatrix}, \tag{19}$$

$$\mathbf{e}_\varsigma \otimes \mathbf{e}_\mathbf{z} = \begin{pmatrix} 0 & 0 & 0 \\ 0 & 0 & 0 \\ 0 & 0 & 1 \end{pmatrix}. \tag{20}$$

Suppose that the deformation takes a particle at location $\mathbb{X}$ with Cartesian coordinates (x, y, z) in the reference configuration to the location Ψ with cylindrical coordinates (r, θ, ς) in the deformed configuration. The deformation gradient is defined as

$$\mathbf{F} = \frac{\partial \Psi}{\partial \mathbb{X}} \Longleftrightarrow \mathrm{d}\Psi = \mathbf{F}\,\mathrm{d}\mathbb{X}, \tag{21}$$

where

$$\mathrm{d}\Psi = \mathrm{d}r\,\mathbf{e}_\mathbf{r} + r\,\mathrm{d}\theta\,\mathbf{e}_\theta + \mathrm{d}\varsigma\,\mathbf{e}_\varsigma,$$

$$\mathrm{d}\mathbb{X} = \mathrm{d}x\,\mathbf{e}_\mathbf{x} + \mathrm{d}y\,\mathbf{e}_\mathbf{y} + \mathrm{d}z\,\mathbf{e}_\mathbf{z}.$$

From (14)–(16), the deformation gradient is written as

$$\begin{aligned}\mathbf{F} &= \frac{\mathrm{d}r}{\mathrm{d}x}\mathbf{e}_\mathbf{r} \otimes \mathbf{e}_\mathbf{x} + r\alpha\mathbf{e}_\theta \otimes \mathbf{e}_\mathbf{y} + \mathbf{e}_\varsigma \otimes \mathbf{e}_\mathbf{z} \\ &= \begin{pmatrix} \frac{\mathrm{d}r}{\mathrm{d}x} & 0 & 0 \\ 0 & r\alpha & 0 \\ 0 & 0 & 1 \end{pmatrix}.\end{aligned} \tag{22}$$

The left Cauchy–Green deformation tensor is $\mathbf{B} = \mathbf{F}\mathbf{F}^\mathrm{T}$, where superscript T denotes transpose [31], so in the present case

$$\begin{aligned}\mathbf{B} &= \lambda_r^2\mathbf{e}_\mathbf{r} \otimes \mathbf{e}_\mathbf{r} + \lambda_\theta^2\mathbf{e}_\theta \otimes \mathbf{e}_\theta + \mathbf{e}_\varsigma \otimes \mathbf{e}_\varsigma \\ &= \begin{pmatrix} \lambda_r^2 & 0 & 0 \\ 0 & \lambda_\theta^2 & 0 \\ 0 & 0 & 1 \end{pmatrix},\end{aligned} \tag{23}$$

where the principal stretches are

$$\lambda_r \triangleq \frac{\mathrm{d}r}{\mathrm{d}x}, \qquad \lambda_\theta \triangleq r\alpha. \tag{24}$$

We assume that both PVDF and PPy are mechanically incompressible. This assumption is based on relevant literature (see [32, 33] for PVDF and [34] for PPy) and will also be justified in part by later experimental validation of the model. For such incompressible materials, the deformation satisfies the constraint that the volume is not changed by the bending after swelling, which means

$$\det \mathbf{F} = \nu, \tag{25}$$

where ν is defined to be the swelling ratio in the different layers,

$$\nu = \begin{cases} \nu_1, & \text{for the reduced PPy layer} \\ 1, & \text{for the PVDF layer} \\ \nu_2, & \text{for the oxidized PPy layer.} \end{cases} \tag{26}$$

From (22), the above equation can be written as

$$\frac{\mathrm{d}r}{\mathrm{d}x} = \frac{\nu}{\alpha r}, \tag{27}$$

implying that λ_r is a function of r, α, and ν. One can integrate (27) and obtain the following equation for the reduced PPy layer:

$$r(x) = \sqrt{r_1^2 + \frac{2}{\alpha}\int_{-h_2}^{x} \nu_1\,\mathrm{d}x}, \qquad -h_2 \leqslant x \leqslant -h_1, \tag{28}$$

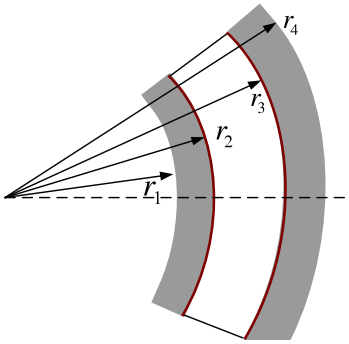

Figure 4. Definition of the bending radii at different locations.

where r_1 is defined as the radius at the inner surface of the beam, as shown in figure 4. Since the swelling is assumed to be uniform over the reduced PPy layer, one can simplify (28) to be

$$r(x) = \sqrt{r_1^2 + \frac{2\nu_1(x + h_2)}{\alpha}}, \qquad -h_2 \leqslant x \leqslant -h_1. \tag{29}$$

Similar equations can be obtained for the PVDF and the oxidized PPy layers:

$$r(x) = \sqrt{r_2^2 + \frac{2(x + h_1)}{\alpha}}, \qquad -h_1 \leqslant x \leqslant h_1, \tag{30}$$

$$r(x) = \sqrt{r_3^2 + \frac{2\nu_2(x - h_1)}{\alpha}}, \qquad h_1 \leqslant x \leqslant h_2, \tag{31}$$

where r_2 is defined as the radius of the boundary between the reduced PPy layer and the PVDF layer, r_3 as the radius of the boundary between the PVDF layer and the oxidized PPy layer, and r_4 as the radius of the outer surface of the beam. The expressions for r_2, r_3, and r_4 are thus

$$r_2 = \sqrt{r_1^2 + \frac{2\nu_1(h_2 - h_1)}{\alpha}}, \tag{32}$$

$$r_3 = \sqrt{r_2^2 + \frac{4h_1}{\alpha}}, \tag{33}$$

$$r_4 = \sqrt{r_3^2 + \frac{2\nu_2(h_2 - h_1)}{\alpha}}. \tag{34}$$

3.3. Stresses

For an isotropic incompressible material, the Cauchy stress tensor depends on the elastic energy density function $\hat{W}$ as follows [31]:

$$\boldsymbol{\sigma} = \frac{2}{\nu}\left[\frac{\partial \hat{W}}{\partial I_1}\mathbf{B} + \frac{\partial \hat{W}}{\partial I_2}(I_1\mathbf{B} - \mathbf{B}^2)\right] - p\mathbf{I}, \tag{35}$$

where $\mathbf{I}$ is the identity matrix. Here p has the interpretation of unknown hydrostatic pressure. I_1 and I_2 are invariants, defined as follows:

$$I_1 = \mathrm{trace}(\mathbf{B}) = 1 + \lambda_r^2 + \lambda_\theta^2 \tag{36}$$

$$I_2 = \tfrac{1}{2}[(\text{trace}(\mathbf{B}))^2 - \text{trace}(\mathbf{B}^2)] = \lambda_r^2 + \lambda_\theta^2 + \lambda_r^2\lambda_\theta^2. \quad (37)$$

Since I_1 and I_2 are functions of λ_r and λ_θ, which are in turn functions of r, α, and ν, it is possible to write

$$\hat{W}(I_1, I_2, \nu) = \tilde{W}(\lambda_r, \lambda_\theta, \nu) = W(r, \alpha, \nu). \quad (38)$$

In the development that follows, each of these is useful in different places.

Combining (35)–(38), one can verify that the principal Cauchy stresses are given by

$$\sigma_{rr} = \frac{\lambda_r}{\nu}\frac{\partial \tilde{W}}{\partial \lambda_r} - p, \quad (39)$$

$$\sigma_{\theta\theta} = \frac{\lambda_\theta}{\nu}\frac{\partial \tilde{W}}{\partial \lambda_\theta} - p. \quad (40)$$

In the absence of body forces, the equilibrium configuration gives

$$\text{div}\sigma = \mathbf{0}, \quad (41)$$

which holds within each of the three layers. From (27) and (39), σ_{rr} is a function of r only. Equation (41) in the $\mathbf{e_r}$ direction then gives [24]

$$\frac{\mathrm{d}\sigma_{rr}}{\mathrm{d}r} + \frac{1}{r}(\sigma_{rr} - \sigma_{\theta\theta}) = 0. \quad (42)$$

Subtracting (40) from (39) and utilizing (38), one has

$$\sigma_{rr} - \sigma_{\theta\theta} = -\frac{r}{\nu}\frac{\partial W}{\partial r}. \quad (43)$$

We use PPy1 to denote the reduced PPy layer, and PPy2 to denote the oxidized PPy layer. Considering the boundary condition $\sigma_{rr}^{\text{PPy1}}(r_1, \alpha, \nu_1) = 0$ and combining (42) and (43), one obtains the following expression for the principal Cauchy radial stress in the reduced PPy layer:

$$\sigma_{rr}^{\text{PPy1}} = \frac{1}{\nu_1}(W^{\text{PPy1}}(r, \alpha, \nu_1) - W^{\text{PPy1}}(r_1, \alpha, \nu_1)). \quad (44)$$

From (43) and (44), the principal Cauchy hoop stress in the reduced PPy layer is

$$\sigma_{\theta\theta}^{\text{PPy1}} = \frac{1}{\nu_1}\left(W^{\text{PPy1}}(r, \alpha, \nu_1) - W^{\text{PPy1}}(r_1, \alpha, \nu_1) + r\frac{\partial W^{\text{PPy1}}}{\partial r}\right). \quad (45)$$

A similar analysis can be used to derive the stresses in the PVDF and the oxidized PPy layer, which results in

$$\sigma_{rr}^{\text{PVDF}} = W^{\text{PVDF}}(r, \alpha) - W^{\text{PVDF}}(r_2, \alpha) + \sigma_{rr}^{\text{PVDF}}(r_2, \alpha), \quad (46)$$

$$\sigma_{rr}^{\text{PPy2}} = \frac{1}{\nu_2}(W^{\text{PPy2}}(r, \alpha, \nu_2) - W^{\text{PPy2}}(r_3, \alpha, \nu_2)) + \sigma_{rr}^{\text{PPy2}}(r_3, \alpha, \nu_2), \quad (47)$$

where $\sigma_{rr}^{\text{PVDF}}(r_2, \alpha)$ and $\sigma_{rr}^{\text{PPy2}}(r_3, \alpha, \nu_2)$ specify the interface values. Note that we have used the assumption of no swelling for the PVDF layer in (46). When there are no fractures or delamination between different layers, σ_{rr} on the interfaces of these layers is continuous, which gives

$$\sigma_{rr}^{\text{PVDF}}|_{r=r_2} = \sigma_{rr}^{\text{PPy1}}|_{r=r_2} =: \sigma_{rr}|_{r_2},$$

$$\sigma_{rr}^{\text{PPy2}}|_{r=r_3} = \sigma_{rr}^{\text{PVDF}}|_{r=r_3} =: \sigma_{rr}|_{r_3}.$$

It follows from (44) and (46) that

$$\sigma_{rr}|_{r_2} = \frac{1}{\nu_1}(W^{\text{PPy1}}(r_2, \alpha, \nu_1) - W^{\text{PPy1}}(r_1, \alpha, \nu_1)),$$

$$\sigma_{rr}|_{r_3} = W^{\text{PVDF}}(r_3, \alpha) - W^{\text{PVDF}}(r_2, \alpha) + \frac{1}{\nu_1}(W^{\text{PPy1}}(r_2, \alpha, \nu_1) - W^{\text{PPy1}}(r_1, \alpha, \nu_1)).$$

Similar to (45), one has the following equations for the hoop stresses in the PVDF layer and the other PPy layer:

$$\sigma_{\theta\theta}^{\text{PVDF}} = \sigma_{rr}^{\text{PVDF}} + r\frac{\partial W^{\text{PVDF}}}{\partial r}, \quad (48)$$

$$\sigma_{\theta\theta}^{\text{PPy2}} = \sigma_{rr}^{\text{PPy2}} + \frac{r}{\nu_2}\frac{\partial W^{\text{PPy2}}}{\partial r}. \quad (49)$$

3.4. Equilibrium

The force and bending moment at any cross section of the beam are zero at equilibrium, which is similar to (5) and (6) but takes different expressions in cylindrical coordinates:

$$\int_{r_1}^{r_2} \sigma_{\theta\theta}^{\text{PPy1}}\mathrm{d}r + \int_{r_2}^{r_3} \sigma_{\theta\theta}^{\text{PVDF}}\mathrm{d}r + \int_{r_3}^{r_4} \sigma_{\theta\theta}^{\text{PPy2}}\mathrm{d}r = 0, \quad (50)$$

$$\int_{r_1}^{r_2} \sigma_{\theta\theta}^{\text{PPy1}} r\,\mathrm{d}r + \int_{r_2}^{r_3} \sigma_{\theta\theta}^{\text{PVDF}} r\,\mathrm{d}r + \int_{r_3}^{r_4} \sigma_{\theta\theta}^{\text{PPy2}} r\,\mathrm{d}r = 0. \quad (51)$$

To capture the nonlinear strain–stress relationship of the PVDF and PPy as the strain increases [22, 23, 29, 30], the energy functions for PVDF and PPy layers are assumed to be of neo-Hookean type [35], which means that they take the general form

$$\hat{W} = \frac{\mu}{2}(I_1 - 3\nu^{2/3}), \quad (52)$$

where μ is the shear modulus. It therefore follows from (24), (27), (36), and (37) that

$$W_{\text{PPy1}}(r, \alpha, \nu_1) = \tfrac{1}{2}\mu_{\text{PPy}}\left[\left(\frac{\nu_1}{\alpha r}\right)^2 + (\alpha r)^2 + 1 - 3\nu_1^{2/3}\right], \quad (53)$$

$$W_{\text{PVDF}}(r, \alpha) = \tfrac{1}{2}\mu_{\text{PVDF}}\left[\left(\frac{1}{\alpha r}\right)^2 + (\alpha r)^2 - 2\right], \quad (54)$$

$$W_{\text{PPy2}}(r, \alpha, \nu_2) = \tfrac{1}{2}\mu_{\text{PPy}}\left[\left(\frac{\nu_2}{\alpha r}\right)^2 + (\alpha r)^2 + 1 - 3\nu_2^{2/3}\right]. \quad (55)$$

The shear moduli μ_i are related to the small strain Young's moduli E_i by $\mu_i = E_i/3$, since the constraint (25) implies a Poisson ratio of 0.5. It is assumed that the energy functions for the PVDF and PPy layers are of neo-Hookean type, because the neo-Hookean model contains the quadratic terms of the mechanical deformation gradient, and it has been adopted to model the nonlinear strain–stress relationships of different smart materials, such as PVDF [36, 37] and ionic polymer–metal composite (IPMC) [38]. Substituting from (53), (54), and (55) into (45), (48), and (49), one obtains

$$\sigma_{\theta\theta}^{\text{PPy1}} = \frac{\mu_{\text{PPy}}}{2\nu_1}\left[\alpha^2(3r^2 - r_1^2) - \frac{\nu_1^2}{\alpha^2}\left(\frac{1}{r^2} + \frac{1}{r_1^2}\right)\right], \quad (56)$$

$$\sigma_{\theta\theta}^{\mathrm{PVDF}} = \frac{\mu_{\mathrm{PVDF}}}{2}\left[\alpha^2(3r^2 - r_2^2) - \frac{1}{\alpha^2}\left(\frac{1}{r^2} + \frac{1}{r_2^2}\right)\right] + \sigma_{rr}|_{r_2}, \tag{57}$$

$$\sigma_{\theta\theta}^{\mathrm{PPy2}} = \frac{\mu_{\mathrm{PPy}}}{2\nu_2}\left[\alpha^2(3r^2 - r_3^2) - \frac{\nu_2^2}{\alpha^2}\left(\frac{1}{r^2} + \frac{1}{r_3^2}\right)\right] + \sigma_{rr}|_{r_3}. \tag{58}$$

From (56)–(58), the left-hand side of (50) is expressed as

$$\begin{aligned}
&\int_{r_1}^{r_2} \sigma_{\theta\theta}^{\mathrm{PPy1}}\mathrm{d}r + \int_{r_2}^{r_3} \sigma_{\theta\theta}^{\mathrm{PVDF}}\mathrm{d}r + \int_{r_3}^{r_4} \sigma_{\theta\theta}^{\mathrm{PPy2}}\mathrm{d}r \\
&= \frac{r_4}{\nu_2}(W^{\mathrm{PPy2}}(r_4, \alpha, \nu_2) - W^{\mathrm{PPy2}}(r_3, \alpha, \nu_2)) \\
&\quad + \sigma_{rr}|_{r_3} \cdot (r_4 - r_3) \\
&\quad + r_3(W^{\mathrm{PVDF}}(r_3, \alpha) - W^{\mathrm{PVDF}}(r_2, \alpha)) + \sigma_{rr}|_{r_2} \cdot (r_3 - r_2) \\
&\quad + \frac{r_2}{\nu_1}(W^{\mathrm{PPy1}}(r_2, \alpha, \nu_1) - W^{\mathrm{PPy1}}(r_1, \alpha, \nu_1)).
\end{aligned} \tag{59}$$

Substituting from (53), (54), and (55) into (59), one finds that the force balance (50) becomes

$$\begin{aligned}
&\frac{\mu_{\mathrm{PPy}}}{2\nu_2}\left[\frac{\nu_2^2}{\alpha^2}\left(\frac{1}{r_4^2} - \frac{1}{r_3^2}\right) + \alpha^2(r_4^2 - r_3^2)\right] + \frac{\mu_{\mathrm{PVDF}}}{2} \\
&\quad \times \left[\frac{1}{\alpha^2}\left(\frac{1}{r_3^2} - \frac{1}{r_2^2}\right) + \alpha^2(r_3^2 - r_2^2)\right] \\
&\quad + \frac{\mu_{\mathrm{PPy}}}{2\nu_1}\left[\frac{\nu_1^2}{\alpha^2}\left(\frac{1}{r_2^2} - \frac{1}{r_1^2}\right) + \alpha^2(r_2^2 - r_1^2)\right] = 0.
\end{aligned} \tag{60}$$

Note that (60) also ensures the boundary condition $\sigma_{rr}^{\mathrm{PPy2}}(r_4, \alpha, \nu_2) = 0$. From (56)–(58), one can find that the moment balance (51) becomes

$$\begin{aligned}
&\frac{\mu_{\mathrm{PPy}}}{\nu_1}\left\{\frac{3}{4}\alpha^2(r_2^4 - r_1^4) + \left(\frac{\nu_1}{\alpha}\right)^2 \ln\frac{r_1}{r_2}\right. \\
&\quad \left. + \frac{1}{2}(r_1^2 - r_2^2)\left[\left(\frac{\nu_1}{\alpha r_1}\right)^2 + (\alpha r_1)^2\right]\right\} \\
&\quad + \mu_{\mathrm{PVDF}}\left\{\frac{3}{4}\alpha^2(r_3^4 - r_2^4) + \frac{1}{\alpha^2}\ln\frac{r_2}{r_3}\right. \\
&\quad \left. + \frac{1}{2}(r_2^2 - r_3^2)\left[\left(\frac{1}{\alpha r_2}\right)^2 + (\alpha r_2)^2\right]\right\} \\
&\quad + \frac{\mu_{\mathrm{PPy}}}{\nu_2}\left\{\frac{3}{4}\alpha^2(r_4^4 - r_3^4) + \left(\frac{\nu_2}{\alpha}\right)^2 \ln\frac{r_3}{r_4}\right. \\
&\quad \left. + \frac{1}{2}(r_3^2 - r_4^2)\left[\left(\frac{\nu_2}{\alpha r_3}\right)^2 + (\alpha r_3)^2\right]\right\} = 0.
\end{aligned} \tag{61}$$

In summary, the problem is now formulated as solving the nonlinear equations (60) and (61) simultaneously by using (32)–(34) to obtain the two unknown variables r_1 and α. These two variables capture the deformed configuration for given swellings ν_1 and ν_2. Note that in the linear elasticity theory-based method, the force balance is automatically satisfied for a symmetrical trilayer structure. However, (60) is required in the nonlinear elasticity theory-based method. Newton's method is applied to numerically solve (60) and (61) with the aid of (32)–(34). Thus a large bending strain model is established for the trilayer conjugated polymer actuator with actuation voltage as the input and bending radius as the output.

4. Experiment

4.1. Materials

The trilayer PPy actuator was fabricated by the Intelligent Polymer Research Institute at the University of Wollongong, Australia [39]. The PPy layers are 30 μm thick, and the PVDF layer is 110 μm thick, which implies that the values of the parameters h_1 and h_2 are 55 μm and 85 μm, respectively. The electrolyte used is 0.05 M tetrabutylammonium hexafluorophosphate ($TBA^+PF_6^-$) in the solvent propylene carbonate (PC). Two actuators of different dimensions were cut from the fabricated sheet. The sizes of the two samples are 12.8×5.0 mm^2 (sample 1) and 31.2×6.0 mm^2 (sample 2) respectively. Each actuator was stored in the electrolyte before experiments for five hours to ensure that the PVDF layer was sufficiently soaked with electrolyte.

4.2. Electrical measurement

A computer equipped with a DS1104 R&D Controller Board (dSPACE Inc.) was used for data acquisition and processing. A trilayer actuator was clamped on one end, where electrical contacts were made using copper tapes. The applied actuation voltage and the corresponding current were measured. Step voltages ranging from 0.2 to 2 V were applied to sample 1, while 0.2–1.4 V were applied to sample 2. The reason for applying the lower maximum step voltage to sample 2 is that the response of sample 2 to voltages higher than 1.4 V is out of the measurement range of the laser sensor.

4.3. Bending measurement

In experiments the beam tip displacement was measured by a laser distance sensor (OADM 20I6441/S14F, Baumer Electric) with resolution of 5 μm, as illustrated in figure 5. One can calculate the curvature κ via the measured displacement $d_0 - d$:

$$\kappa = \frac{1}{r} = \frac{2(d_0 - d)}{(d_0 - d)^2 + l^2}, \tag{62}$$

where l is the distance between the clamped end and the laser incident point when the beam is at rest.

5. Results and discussion

The relationships between the input voltages and the transferred charges for the two different samples are shown in figure 6. The constant k_1 in (2) can be determined from the experimental data; it is found to be 0.0936 C V^{-1} and 0.1801 C V^{-1}, respectively, for samples 1 and 2. The value of the swelling-to-charge ratio κ_2 was finely tuned, based on the reported value in [17], to be 1.12×10^{-10} m^3 C^{-1} in order to make the model prediction fit the experimental data. The small strain Young's moduli of PPy and PVDF were taken to be 60 and 612 MPa [40].

The predictions of r_1 and α on the basis of (60) and (61) are shown in figures 7–10 for the two samples. The experimental data for the bending radii are also compared with the predictions of r_1 in figures 7 and 8 for the two samples.

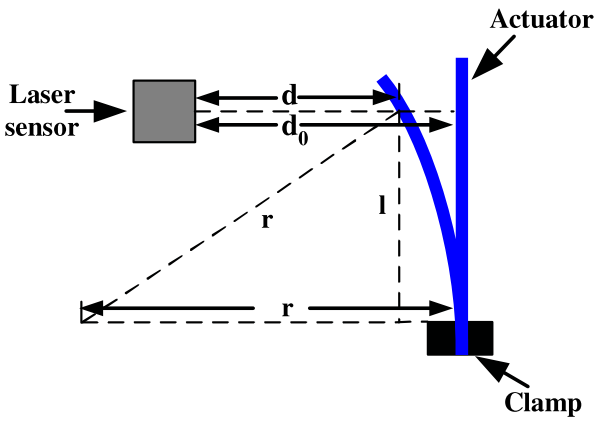

Figure 5. Geometric relationship between the beam curvature and the tip displacement.

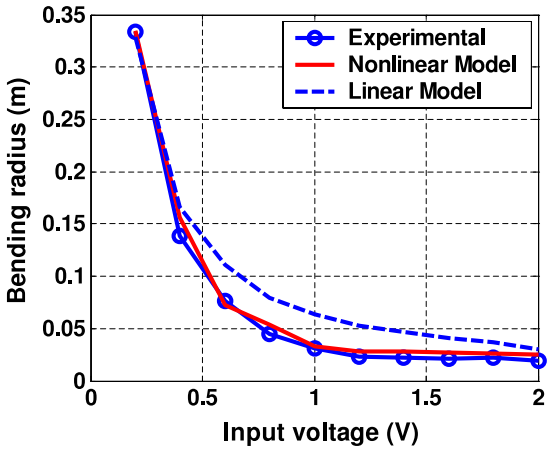

Figure 7. Quasi-static bending under different actuation voltages for sample 1 (13 mm × 5 mm).

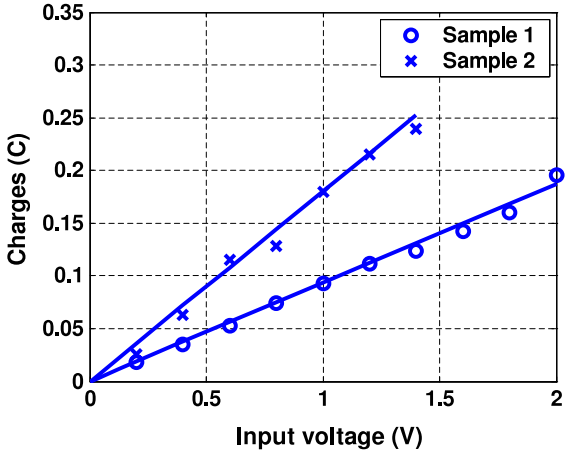

Figure 6. The relationships between the input voltages and the transferred charges for the two different samples.

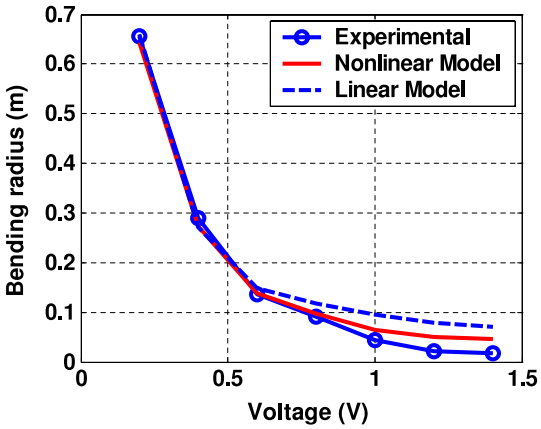

Figure 8. Quasi-static bending under different actuation voltages for sample 2 (33 mm × 6 mm).

The predictions by the linear model (10) are also shown in the figures for comparison purposes. Note that the same parameters are used in the linear model. It can be seen that when the applied voltage is low (i.e., the volume changes of the PPy layers are small), the predictions by the linear and nonlinear models can both fit the experimental data. But as the applied voltage increases, the prediction of the linear model deviates significantly from the experimental data. On the other hand, the nonlinear model still shows good fitting, thus demonstrating the effectiveness of the nonlinear model over a larger deformation range. Note that the bending radius of the beam will decrease and approach zero as the voltage applied on the conjugated polymer increases, which implies that the curves of the experiments and model outputs will approach each other asymptotically for high actuation voltages. This accounts for the apparent decreased deviation of the linear model from both the experimental measurement and the nonlinear model at high voltages in figures 7 and 8.

Based on the obtained values of r_1 and α, one can calculate r_2, r_3, and r_4 by using (32)–(34). Furthermore, the thickness of PPy layers can be obtained by calculating $r_2 - r_1$ and $r_4 - r_3$ at different actuation voltages. Similarly, the thickness of

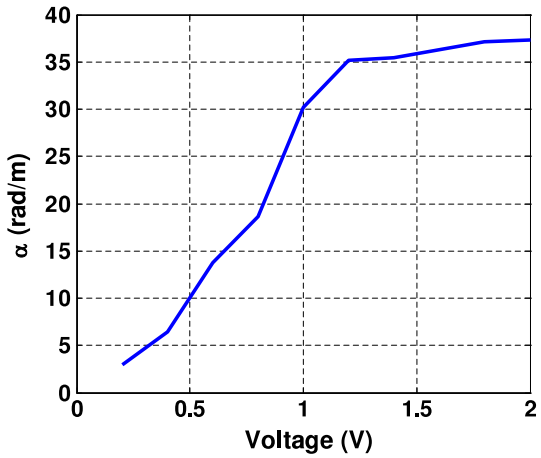

Figure 9. Computational results on the change of α versus the applied voltage for sample 1 (13 mm × 5 mm).

the PVDF layer is obtained through $r_3 - r_2$. The results for sample 1 are shown in figures 11 and 12. When the voltage increases, the thickness of the reduced PPy layer will decrease and that of the oxidized PPy layer will increase for the oxidized

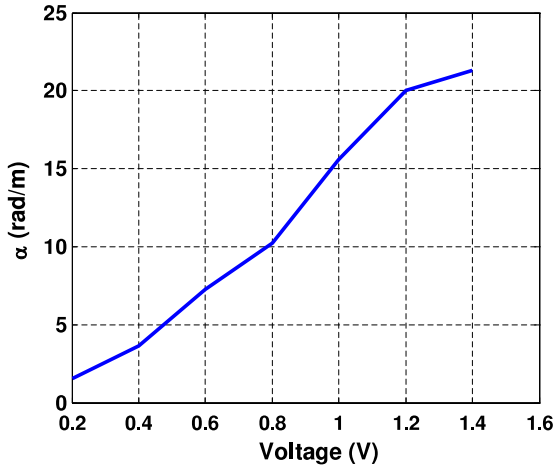

Figure 10. Computational results on the change of α versus the applied voltage for sample 2 (33 mm $\times$ 6 mm).

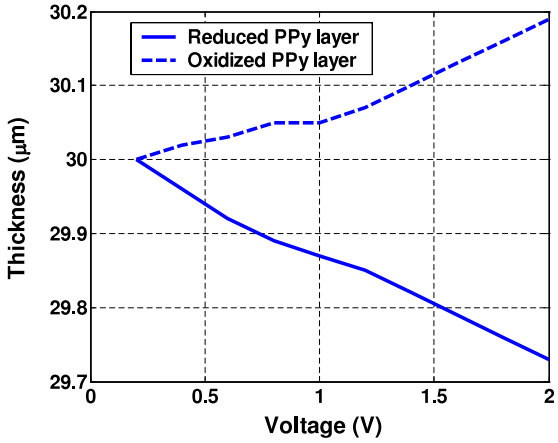

Figure 11. Computational results on the changes of thickness of the PPy layers with the applied voltage for sample 1.

PPy layer. The percentage change at 2 V is -0.83% for the reduced PPy layer and 0.67% for the oxidized PPy layer. The thickness of the PVDF layer is decreasing, but at a slower rate when the input voltage is increasing. The percentage change at 2 V is 0.21%. Note that these results provide an interesting insight into the deformed configuration. Such information is not available from linear models, since the latter assume fixed thickness throughout the deformation.

6. Conclusions and future work

A nonlinear elasticity theory-based framework is proposed to analyze the bending configuration of a trilayer conjugated polymer beam under different actuation voltages. Neo-Hookean type strain energy functions are used for the PPy and PVDF layers of the trilayer beam to capture the nonlinearity under large deformations. For a constant actuation voltage, the swelling of each PPy layer is determined by the amount of transferred ions. The bending configuration at the equilibrium is obtained by solving the force and moment balance equations simultaneously. Experimental results have validated the effectiveness of the proposed nonlinear model. The method further provides insight into the deformation details, such as the change of layer thickness.

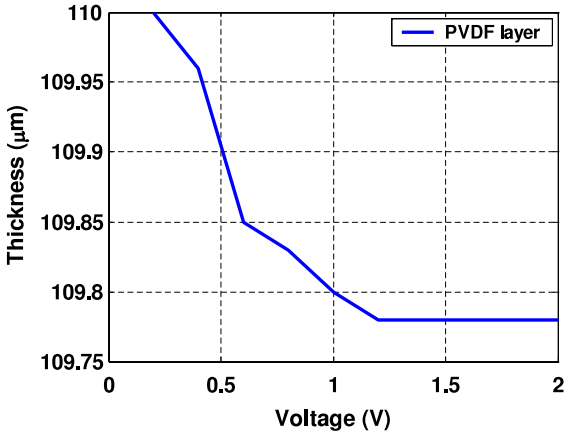

Figure 12. Computational results on the changes of thickness of the PVDF layer with the applied voltage for sample 1.

A similar analysis can be used for some other EAPs that involve a local volume change (swelling). This is important for many applications involving large deformations, when the elastic modulus of the material already becomes nonlinear and linear elasticity analysis does not hold. For more complicated actuator configurations, this would typically require a finite element treatment.

In this paper the analysis was focused on quasi-static actuation. This will be extended to accommodate dynamic voltage inputs in future work. We will also investigate the incorporation of nonlinear electrical dynamics [41] into the current framework.

Acknowledgments

The work of Y Fang and X Tan was supported in part by an NSF CAREER grant (ECCS 0547131) and MSU IRGP (05-IRGP-418), and the work of T Pence was supported by an NSF grant (CMMI 0510600). The authors would like to thank Professor Gürsel Alici for providing the PPy samples. Useful discussions with Mr Hua Deng from the Department of Mechanical Engineering at Michigan State University are greatly appreciated.

References

[1] Smela E, Inganas O and Lundstrom I 1995 Controlled folding of micro-size structures *Science* **268** 1735–8
[2] Jager E W H, Inganas O and Lunstrom I 2000 Microrobots for micrometer-size objects in aqueous media: potential tools for single cell manipulation *Science* **288** 2335–8
[3] Zhou J, Chan H, To T, Lai K and Li W J 2004 Polymer MEMS actuators for underwater micromanipulation *IEEE/ASME Trans. Mechatronics* **9** 334–42
[4] Mazzoldi A and De Rossi D 2000 Conductive-polymer-based structures for a steerable catheter *Smart Structures and Materials 2000: Electroactive Polymer Actuators and Devices*; *Proc. SPIE* **3987** 273–80

[5] Chen Z and Tan X 2007 A dynamic model for ionic polymer-metal composite sensors *Smart Mater. Struct.* **16** 1477–88
[6] Chen Z, Shen Y, Xi N and Tan X 2007 Integrated sensing for ionic polymer-metal composite actuators using PVDF thin films *Smart Mater. Struct.* **16** S262–71
[7] Baughman R 1996 Conducting polymer artificial muscles *Synth. Met.* **78** 339–53
[8] Smela E 2003 Conjugated polymer actuators for biomedical applications *J. Adv. Mater.* **15** 481–94
[9] Wallace G G, Spinks G M, Kane-Maguire L and Teasdale P R 2003 *Conductive Electroactive Polymers: Intelligent Materials Systems* 2nd edn (Boca Raton, FL: CRC Press LLC)
[10] Della Santa A, De Rossi D and Mazzoldi A 1997 Characterization and modelling of a conducting polymer muscle-like linear actuator *Smart Mater. Struct.* **6** 23–34
[11] Kaneko M and Kaneto K 1999 Electrochemomechanical deformation in polyaniline and poly(o-methoxyaniline) *Synth. Met.* **102** 1350–3
[12] Wu Y, Zhou D, Spinks G, Innis P and Wallace G 2005 Titan: a conducting polymer based microfluidic pump *Smart Mater. Struct.* **14** 1511–6
[13] Immerstrand C, Peterson K H, Magnusson K-E, Jager E W H, Krogh M, Skoglund M, Selbing A and Inganas O 2002 Conjugated-polymer micro-and milliactuators for biological applications *Mater. Res. Soc. Bull.* **27** 461–4
[14] Smela E, Kallenbach M and Holdenried J 1999 Electrochemically driven polypyrrole bilayers for moving and positioning bulk micromachined silicon plates *Microelectromech. Syst.* **8** 373–83
[15] Alici G, Mui B and Cook C 2006 Bending modeling and its experimental verification for conducting polymer actuators dedicated to manipulation applications *Sensors Actuators* A **126** 396–404
[16] Fang Y, Tan X and Alici G 2008 Robust adaptive control of conjugated polymer actuators *IEEE Trans. Control Syst. Technol.* **14** 600–12
[17] Madden J D W 2000 Conducting polymer actuators *PhD Thesis* MIT
[18] Pei Q and Inganäs O 1992 Electrochemical applications of the bending beam method. 1. Mass transport and volume changes in polypyrrole during redox *J. Phys. Chem.* **96** 10507–14
[19] Christophersen M, Shapiro B and Smela E 2006 Characterization and modeling of PPy bilayer microactuators. Part 1. Curvature *Sensors Actuators* B **115** 596–609
[20] Madden P G A 2003 Development and modeling of conducting polymer actuators and the fabrication of a conducting polymer based feedback loop *Phd Thesis* MIT
[21] Metza P, Alici G and Spinks G 2006 A finite element model for bending behaviour of conducting polymer electromechanical actuators *Sensors Actuators* A **130** 1–11
[22] Madden J D, Rinderknecht D, Anquetil P A and Hunter I W 2007 Creep and cycle life in polypyrrole actuators *Sensors Actuators* A **133** 210–7
[23] Otero T F, Cascales J J L and Arenas G V 2007 Mechanical characterization of free-standing polypyrrole film *Mater. Sci. Eng.* C **27** 18–22
[24] Tsai H, Pence T J and Kirkinis E 2004 Swelling induced finite strain flexure in a rectangular block of an isotropic elastic material *J. Elast.* **75** 69–89
[25] Bull R, Fan F-R and Bard A 1982 Polymer films on electrodes *J. Electrochem. Soc.* **129** 1009–15
[26] Franklin G F, Powell J D and Emami-Naeini A 2006 *Feedback Control of Dynamic Systems* 5th edn (Upper Saddle River, NJ: Pearson Education)
[27] Gere J M and Timoshenko S P 1990 *Mechanics of Materials* (Boston, MA: PWS-KENT)
[28] Fang Y, Tan X, Shen Y, Xi N and Alici G 2008 A scalable model for trilayer conjugated polymer actuators and its experimental validation *Mater. Sci. Eng.* C **28** 421–8
[29] Wang D W, Tzou H S and Lee H-J 2004 Control of nonlinear electro/elastic beam and plate systems (finite element formulation and analysis) *J. Vib. Acoust.* **126** 63–70
[30] Sathiyanarayan S, Sivakumar S M and Rao C L 2006 Nonlinear and time-dependent electromechanical behavior of polyvinylidene fluoride *Smart Mater. Struct.* **15** 767–81
[31] Bonet J and Wood R 1997 *Nonlinear Continuum Mechanics for Finite Element Analysis* (Cambridge: Cambridge University Press)
[32] Mano J, Lopes J, Silva R and Brostow W 2003 Creep of PVDF monofilament sutures: service performance prediction from short-term tests *Polymer* **44** 4293–300
[33] Castro M, Carrot C and Prochazka F 2004 Experimental and theoretical description of low frequency viscoelastic behaviour in immiscible polymer blends *Polymer* **45** 4095–104
[34] Therkelsen S 2005 Constitutive modeling of active polymers *Master Thesis* MIT
[35] Treloar L 1975 *The Physics of Rubber Elasticity* (Oxford: Clarendon Press)
[36] Batra R C and Geng T S 2001 Enhancement of the dynamic buckling load for a plate by using piezoceramic actuators *Smart Mater. Struct.* **10** 925–33
[37] Yang J S and Batra R C 1995 A second-order theory for piezoelectric materials *J. Acoust. Soc. Am.* **97** 280–8
[38] Nemat-Nasser S and Wu Y 2006 Tailoring the actuation of ionic polymercmetal composites *Smart Mater. Struct.* **15** 909–23
[39] Wu Y, Alici G, Spinks G M and Wallace G G 2006 Fast trilayer polypyrrole bending actuators for high speed applications *Synth. Met.* **156** 1017–22
[40] Alici G, Metz P and Spinks G M 2006 A methodology towards geometry optimization of high performance polypyrrole (PPy) actuators *Smart Mater. Struct.* **15** 243–52
[41] Fang Y, Tan X and Alici G 2008 Redox level-dependent impedance model for conjugated polymer actuators *Sensors Actuators* B **132** 182–90